IPPP/08/52
DCPT/08/104
October 27, 2008

Diffractive dissociation re-visited for predictions at the LHC

E.G.S. Luna[a], V.A. Khoze[a,b], A.D. Martin[a] and M.G. Ryskin[a,b]

[a] Institute for Particle Physics Phenomenology, University of Durham, Durham, DH1 3LE
[b] Petersburg Nuclear Physics Institute, Gatchina, St. Petersburg, 188300, Russia

Abstract

We describe the formalism, and present the results, for a triple-Regge analysis of the available pp and $p\bar{p}$ high-energy data which explicitly accounts for absorptive corrections. In particular, we allow for the gap survival probability, S^2, in single proton diffractive dissociation. Since for pp scattering the value of S^2 is rather small, the triple-Pomeron vertex obtained in this analysis is larger than that obtained in the old analyses where the suppression caused by the absorptive corrections was implicitly included in an *effective* vertex. We show that the *bare* triple-Pomeron coupling that we extract from the pp and $p\bar{p}$ data is consistent with that obtained in a description of the $\gamma p \to J/\psi + Y$ HERA data. The analyses of the data prefer a zero slope, corresponding to the small size of the bare vertex, giving the hope of a smooth matching to the perturbative QCD treatment of the triple-Pomeron coupling.

1 Motivation

The total and elastic proton-proton cross sections are usually described in terms of an eikonal model [1]. The advantage of using an eikonal framework is that it automatically satisfies s-channel unitarity, which follows once we include the elastic rescattering of the interacting

particles. Furthermore, the Good-Walker formalism [2] allows the possibility of excited proton states occurring in the intermediate state. In this way we include low-mass diffractive dissociation. It was demonstrated in [3] that a two-channel eikonal is sufficient to capture the main features of this dissociation (provided, of course, we are not interested in the production of a particular resonant state), see also [4].

On the other hand, high-mass (M) diffractive dissociation is described in terms of the triple-Regge formalism, where the differential cross section, $d\sigma/dtdM^2$, is driven by the triple-Regge couplings $g_{R_1R_2R_3}$. The values of these couplings were determined from the data available in triple-Regge domain in the 1970s; see, for example [5, 6, 7]. However, these early analyses did not allow for absorptive corrections, which are sizeable in hadron-hadron collisions. Therefore, the old triple-Regge couplings must be regarded, not as the bare vertices, but as effective couplings embodying absorptive effects. It was pointed out in Ref. [8] that the original *bare* triple-Pomeron vertex may be about three times larger than the *effective* coupling which is obtained with the neglect of absorptive corrections. However, absorptive effects are very sensitive to the t-slope of the triple-Reggeon vertices and in the 1970s it was "impossible to determine the exact values of the *bare* triple-Pomeron coupling" [8]; the accuracy and energy range covered by the data were insufficient. So the results of the triple-Regge analyses were presented in the form of *effective* couplings. This leads to a problem, since the absorptive effects are not constant factors, but depend on the energy and the type of diffractive process. Since the inelastic cross section expected at the LHC is more than twice as large as that observed at fixed target and CERN-ISR energies, we cannot use the results of the old triple-Regge analyses to predict the diffractive effects at the LHC[1]. It is therefore necessary to perform a new triple-Regge analysis that includes the absorptive effects explicitly. Here we present the first analysis of the available diffractive (and elastic) data in the CERN-ISR – Tevatron region in which the absorptive corrections are systematically included. The absorptive corrections are calculated in terms of a two-channel eikonal model fitted to describe the total and elastic differential cross section data for pp and $p\bar{p}$ scattering.

At the moment, the energy behaviour of the scattering amplitude may be consistently described by two different scenarios for the asymptotic regime [11]. One is called the *weak coupling* of the Pomerons. In this case, at very high energy, the cross sections tend to the universal constant value

$$\sigma_{\rm tot} \to \text{constant} \qquad \text{as} \quad s \to \infty. \tag{1}$$

In order not to violate unitarity, the triple-Pomeron coupling must vanish with vanishing transverse momentum transferred through the Pomeron [12]

$$g_{3P} \propto q_t^2 \qquad \text{as} \quad q_t \to 0. \tag{2}$$

Another possibility is called the *strong coupling* scenario [13]. Here, at a very high energies, the cross sections grows as

$$\sigma_{\rm tot} \propto (\ln s)^\eta \qquad \text{with} \qquad 0 < \eta \leq 2, \tag{3}$$

[1] Already, in order to describe data up to the Tevatron energy, Goulianos and Montanha [9] found it necessary to restore unitarity by renormalising the "Pomeron flux" [10]. This mimics to some extent the absorptive effects.

and the bare vertex

$$g_{3P}|_{q_t\to 0} \quad \to \quad \text{constant.} \tag{4}$$

The present data are usually described within the Froissart-like limit of the second scenario (with $\eta = 2$). However to reach asymptotics we need **very** high energy – the energy at which the slope of the elastic amplitude, $B = B_0 + \alpha'_P \ln(s)$ is dominated by the second term, that is when $\alpha'_P \ln(s) \gg B_0$. This is far beyond the energies available at present. Another possibility, to distinguish between the *weak* and *strong* approaches, is to study the q_t dependence of the bare triple-Pomeron vertex. Thus, it is important to extract the *bare* vertex before its behaviour is affected by absorptive corrections.

This paper is devoted to a detailed analysis of "soft" scattering data using, in turn, the *strong* and *weak* triple-Pomeron coupling behaviours. In Section 2 we recall the Good-Walker formalism for the two-channel eikonal model, in Section 3 we briefly describe the parametrisation used to calculate the absorptive corrections for the triple-Reggeon cross sections and demonstrate that this parametrisation is consistent with the available data on the differential elastic ($d\sigma_{\rm el}/dt$) and total cross sections. Next, in Section 4, we give the formulae for the inclusive cross section, $M^2 d\sigma/dt dM^2$, in the triple-Regge region which incorporates the screening corrections caused by the two-channel eikonal. The results of our triple-Regge analyses of $pp \to pX$ and $\bar{p}p \to \bar{p}X$ data are presented in Section 5. We perform fits using both the strong and weak triple-Pomeron coupling. We find that the data favour the former ansatz. In Section 6 we discuss the description of the data for inelastic diffractive J/ψ photoproduction, $\gamma p \to J/\psi + Y$, obtained at HERA. We find that the J/ψ HERA data again favour the strong triple-Pomeron coupling scenario. In Section 7 we present our conclusions.

2 Résumé of the eikonal formalism

2.1 Single-channel eikonal model

First, we briefly recall the relevant features of the single-channel eikonal model. That is we focus on elastic unitarity. Then "disc T" is simply the discontinuity of the pp scattering amplitude T across the two-particle s-channel cut. At high energies we have a sizeable inelastic component. The s-channel unitarity relation is diagonal in the impact parameter, b, basis, and may be written

$$2{\rm Im}\, T_{\rm el}(s,b) = |T_{\rm el}(s,b)|^2 + G_{\rm inel}(s,b) \tag{5}$$

with

$$\sigma_{\rm tot} = 2\int d^2b\, {\rm Im}\, T_{\rm el}(s,b) \tag{6}$$

$$\sigma_{\rm el} = \int d^2b\, |T_{\rm el}(s,b)|^2 \tag{7}$$

$$\sigma_{\rm inel} = \int d^2b\, \left[2{\rm Im}\, T_{\rm el}(s,b) - |T_{\rm el}(s,b)|^2\right]. \tag{8}$$

These equations are satisfied by

$$\mathrm{Im}T_{\rm el}(s,b) \;=\; 1-\mathrm{e}^{-\Omega/2} \tag{9}$$

$$\sigma_{\rm el}(s,b) \;=\; (1-\mathrm{e}^{-\Omega/2})^2, \tag{10}$$

$$\sigma_{\rm inel}(s,b) \;=\; 1-\mathrm{e}^{-\Omega}, \tag{11}$$

where $\Omega(s,b) \geq 0$ is called the opacity (optical density) or eikonal[2]. From (11), we see that $\exp(-\Omega(s,b))$ is the probability that no inelastic scattering occurs.

The opacity corresponding to an individual Regge pole $i = R$ or P takes the form

$$\Omega_i(s,b) \;=\; \frac{1}{\pi}\int d^2q_t\; A_i(s,q_t)e^{i\vec{q}_t\cdot\vec{b}} \;=\; \frac{\beta_i(0)^2(s/s_0)^{\alpha_i(0)-1}}{B_i}\, e^{-b^2/4B_i}, \tag{12}$$

where $q_t^2 = -t$, and where the contribution to the amplitude from Reggeon i exchange is[3]

$$A_i(s,q_t) \;=\; \eta_i\beta_i(0)^2e^{r_it}(s/s_0)^{\alpha_i(t)-1}, \tag{13}$$

where the t behaviour of the Reggeon-proton vertex is taken to have the exponential form

$$\beta_i(t) \;=\; \beta_i(0)\exp(r_it/2). \tag{14}$$

Thus, for a linear trajectory

$$\alpha_i = \alpha_i(0) + \alpha_i't, \tag{15}$$

the t-slope of the amplitude A_i is given by

$$B_i \;=\; r_i \;+\; \alpha_i'\,\ln(s/s_0). \tag{16}$$

For Regge exchange with signature ±1, the factor η_i in eq. (13) is

$$\eta_i \;=\; \frac{-(1\pm e^{-i\pi\alpha_i})}{\sin\pi\alpha_i}. \tag{17}$$

Although we take exponential forms for the exchange of the secondary Reggeons, we choose, as in Ref. [14], a power-like form for the proton-Pomeron vertex

$$\beta_P(t) \;=\; \frac{\beta_P(0)}{(1-t/a_1)(1-t/a_2)}. \tag{18}$$

Also, to improve the description of the low $|t|$ region, we follow Anselm and Gribov [16] and include pion-loop insertions[4] in Pomeron exchange which results in a non-linear form of the Pomeron trajectory

$$\alpha_P(t) \;=\; \alpha_P(0) \;+\; \alpha_P't \;-\; \frac{\beta_\pi^2m_\pi^2}{32\pi^3}\,h\left(\frac{4m_\pi^2}{|t|}\right), \tag{19}$$

[2]Sometimes $\Omega/2$ is called the eikonal; for simplicity we omit the real part of $T_{\rm el}$. At high energies, the ratio $\mathrm{ReT_{el}/ImT_{el}}$ is small, and can be evaluated via a dispersion relation.

[3]Note that, unlike [3, 14, 15], here we use the normalisation $\sigma_i^{\rm tot} = 4\pi\mathrm{Im}\eta_i\ \beta_i(0)^2(s/s_0)^{\alpha_i(0)-1}$, rather than $\sigma_i^{\rm tot} = \mathrm{Im}\eta_i\ \beta_i(0)^2(s/s_0)^{\alpha_i(0)-1}$. That is, as compared to our previous papers, here all the coupling constants (β_i and g_{iij}) are decreased by a factor $\sqrt{4\pi}$.

[4]Note that, in (20) below, we have corrected the misprint which occurs in the published version of [16].

where

$$h(\tau) \;=\; \frac{4}{\tau}\,F_\pi^2(t)\,\left[2\tau \;-\; (1+\tau)^{3/2}\,\ln\left(\frac{\sqrt{1+\tau}+1}{\sqrt{1+\tau}-1}\right) \;+\; \ln\frac{m^2}{m_\pi^2}\right], \tag{20}$$

with $\tau = 4m_\pi^2/|t|$ and $m = 1$ GeV. The coefficient β_π^2 specifies the $\pi\pi$ total cross section, and $F_\pi(t)$ is the form factor of the pion-Pomeron vertex. The coefficient $\beta_\pi^2 m_\pi^2/32\pi^3$ in (19) is small[5], but due to the tiny scale m_π the t dependence of $h(\tau)$ is steep and non-linear. It has an important effect on the local slope, $d(\ln d\sigma_{\rm el}/dt)/dt$, of the elastic cross section. For the results that we obtain below for the Pomeron trajectory, $\alpha_P(t)$, it is important to note that expression (20) for $h(\tau)$ has been renormalised [16], such that

$$h(\tau) \;=\; h_\pi(\tau) \;-\; h_\pi(0) \tag{21}$$

where $h_\pi(\tau)$ denotes the full pion-loop contribution. Further discussion of the pion-loop contribution can be found in Ref. [14].

Finally, the total opacity is given by the sum of all the allowed Regge exchanges

$$\Omega \;=\; \sum_{i=P,R}\Omega_i. \tag{22}$$

In the present simplified analysis we neglect the real part of the amplitude, since our goal is to investigate the role of the absorptive effect which is caused essentially by the imaginary part of the amplitude, that is by the real part of the opacity. Therefore, the values of the couplings $\beta_i(0)$, that we quote in Table 1 below, are actually $\mathrm{Im}(\eta_i\beta_i(0))$, where the η_i are the signature factors of (17).

2.2 Inclusion of low-mass diffractive dissociation

So much for elastic diffraction. Now we turn to inelastic diffraction, which is a consequence of the *internal structure* of hadrons. This is simplest to describe at high energies, where the lifetime of the fluctuations of a fast hadron is large, $\tau \sim E/m^2$, and during these time intervals the corresponding Fock states can be considered as 'frozen'. Each hadronic constituent can undergo scattering and thus destroy the coherence of the fluctuations. As a consequence, the outgoing superposition of states will be different from the incident particle, and will most likely contain multiparticle states, so we will have *inelastic*, as well as elastic, diffraction.

To discuss inelastic diffraction, it is convenient to follow Good and Walker [2], and to introduce states ϕ_k which diagonalize the T matrix. Such eigenstates only undergo elastic scattering. Since there are no off-diagonal transitions,

$$\langle\phi_j|T|\phi_k\rangle = 0 \qquad \text{for } j \neq k, \tag{23}$$

[5]We use the additive quark model relation $\beta_\pi(\equiv g_{\pi\pi P}) = \frac{2}{3}\beta_P(0)$.

a state k cannot diffractively dissociate into a state j. We have noted that this is not, in general, true for hadronic states, which are not eigenstates of the S-matrix, that is of T. To account for the internal structure of the hadronic states, we have to enlarge the set of intermediate states, from just the single elastic channel, and to introduce a multichannel eikonal. We will consider such an example below, but first let us express the cross section in terms of the probability amplitudes F_k of the hadronic process proceeding via the various diffractive eigenstates[6] ϕ_k.

Let us denote the orthogonal matrix which diagonalizes $\mathrm{Im}\, T$ by a, so that

$$\mathrm{Im}\, T \;=\; aFa^T \qquad \text{with} \qquad \langle\phi_j|F|\phi_k\rangle \;=\; F_k\,\delta_{jk}. \tag{24}$$

Now consider the diffractive dissociation of an arbitrary incoming state

$$|j\rangle \;=\; \sum_k a_{jk}\,|\phi_k\rangle. \tag{25}$$

The elastic scattering amplitude for this state satisfies

$$\langle j|\mathrm{Im}\; T|j\rangle \;=\; \sum_k |a_{jk}|^2\,F_k \;=\; \langle F\rangle, \tag{26}$$

where $F_k \equiv \langle\phi_k|F|\phi_k\rangle$ and where the brackets of $\langle F\rangle$ mean that we take the average of F over the initial probability distribution of diffractive eigenstates. After the diffractive scattering described by T_{fj}, the final state $|f\rangle$ will, in general, be a different superposition of eigenstates from that of $|j\rangle$, which was shown in (25). At high energies we may neglect the real parts of the diffractive amplitudes. Then, for cross sections at a given impact parameter b, we have

$$\begin{aligned}
\frac{d\sigma_{\rm tot}}{d^2b} &= 2\,\mathrm{Im}\langle j|T|j\rangle \;=\; 2\sum_k |a_{jk}|^2\,F_k \;=\; 2\langle F\rangle \\
\frac{d\sigma_{\rm el}}{d^2b} &= |\langle j|T|j\rangle|^2 \;=\; \left(\sum_k |a_{jk}|^2\,F_k\right)^2 \;=\; \langle F\rangle^2 \\
\frac{d\sigma_{\rm el\,+\,SD}}{d^2b} &= \sum_k |\langle\phi_k|T|j\rangle|^2 \;=\; \sum_k |a_{jk}|^2\,F_k^2 \;=\; \langle F^2\rangle.
\end{aligned} \tag{27}$$

It follows that the cross section for the single diffractive dissociation of a proton,

$$\frac{d\sigma_{\rm SD}}{d^2b} \;=\; \langle F^2\rangle \;-\; \langle F\rangle^2, \tag{28}$$

is given by the statistical dispersion in the absorption probabilities of the diffractive eigenstates. Here the average is taken over the components k of the incoming proton which dissociates. If the averages are taken over the components of both of the incoming particles, then in (28) we must introduce a second index on F, that is F_{ik}, and sum over k and i. In this case the sum is the cross section for single and double dissociation.

[6]The exponent $\exp(-\Omega_k)$ describes the probability that the diffractive eigenstate ϕ_k is not absorbed in the interaction. Later we will see that the rapidity gap survival factors, S^2, can be described in terms of such eikonal exponents.

3 Description of the elastic data

In preparation for the triple-Regge analysis of the data for high-mass diffraction, we first perform a two-channel eikonal fit to all the high-energy pp and $p\bar{p}$ total cross section data above $\sqrt{s} = 10$ GeV and to the elastic differential scattering cross section for pp at $\sqrt{s} = 31$, 53 and 62 GeV, and for $p\bar{p}$ at $\sqrt{s} = 31$, 53, 62, 546 and 1800 GeV. We use total cross section data sets compiled by the Particle Data Group [17] and differential cross section data sets from the references [18] (ISR), [19] ($Sp\bar{p}S$) and [20] (Tevatron), see the review in Ref. [21]. The statistic and systematic errors of all scattering quantities have been added in quadrature.

We introduce a parameter γ to define the two diffractive eigenstates k of the eikonal model, such that their couplings to the Pomeron are

$$\beta_{P,k}(t) \;=\; (1 \pm \gamma)\beta_P(t), \tag{29}$$

where the proton wave function $|p\rangle = (|+\rangle + |-\rangle)/\sqrt{2}$, see Ref. [14]. The CERN-ISR measurements of the excitations into particular channels ($N\pi$, $N\pi\pi$, ΛK etc.) with $M < 2.5$ GeV [22] correspond to a cross section for low-mass diffraction of[7]

$$\sigma_{\rm SD}^{{\rm low}M} \simeq 2 \text{ mb} \qquad \text{at } \sqrt{s} = 31 \text{ GeV}. \tag{30}$$

This value corresponds to $\gamma \simeq 0.55$, which we take in this analysis.

We describe the pp and $p\bar{p}$ total and elastic cross section data in terms of Pomeron, and positive (f_2, a_2) and negative (ω, ρ) signature Regge exchange. The *positive* signature secondary Reggeons, f_2 and a_2, are taken to lie on an exchange-degenerate linear trajectory with intercept $\alpha_+(0)$ and coupling[8] to the proton of parametric form

$$\beta_+(t) \;=\; \beta_+(0)\, \exp(r_+ t/2), \tag{31}$$

see (14). Similarly, the exchange-degenerate *negative* signature pair (ω, ρ) are described by parameters $\alpha_-(0)$, $\beta_-(0)$ and r_-. The slopes, α'_+, α'_-, of the secondary Reggeon linear trajectories are fixed at 0.9 GeV^{-2}. On the other hand, the Pomeron coupling and trajectory are taken to have parametric forms given by (18) and (19), respectively.

The values of the Regge parameters determined by the global fit are listed in Table 1. The fit has $\chi^2/\text{DoF} = 259/(325-11) = 0.83$. The description of σ_{tot} and $d\sigma/dt$ is displayed in Fig. 1, where the solid (dashed) curves correspond to $p\bar{p}$ (pp) scattering. The total cross section at LHC is predicted[9] to be $\sigma_{\rm tot} = 94.8$ mb.

[7] Here, and in what follows, the value of $\sigma_{\rm SD}$ accounts for dissociation of both colliding particles.

[8] If we assume the additive-quark-model relation, $\beta(f_2) = 3\beta(a_2)$, then the coupling $\beta(f_2) = \sqrt{9/10}\ \beta_+$.

[9] As expected, the inclusion of absorption reduces the value of the cross section predicted at the LHC energy. Indeed, if the high-mass diffractive absorptive effects were also included then the total cross section would be further reduced to about 90 mb [3, 23], see also [24, 4]. The present model also predicts an elastic pp differential cross section at the LHC energy with a diffractive dip at $-t \simeq 0.4\text{GeV}^2$. However, for this prediction to be reliable we must await the inclusion of the high-mass absorptive effects in the elastic analysis [23]. An earlier analysis [3], which included high-mass diffraction phenomenologically, showed that, at the LHC energy, the dip occurred at larger $-t$ and that the elastic cross section was smooth in the region shown in Fig. 1.

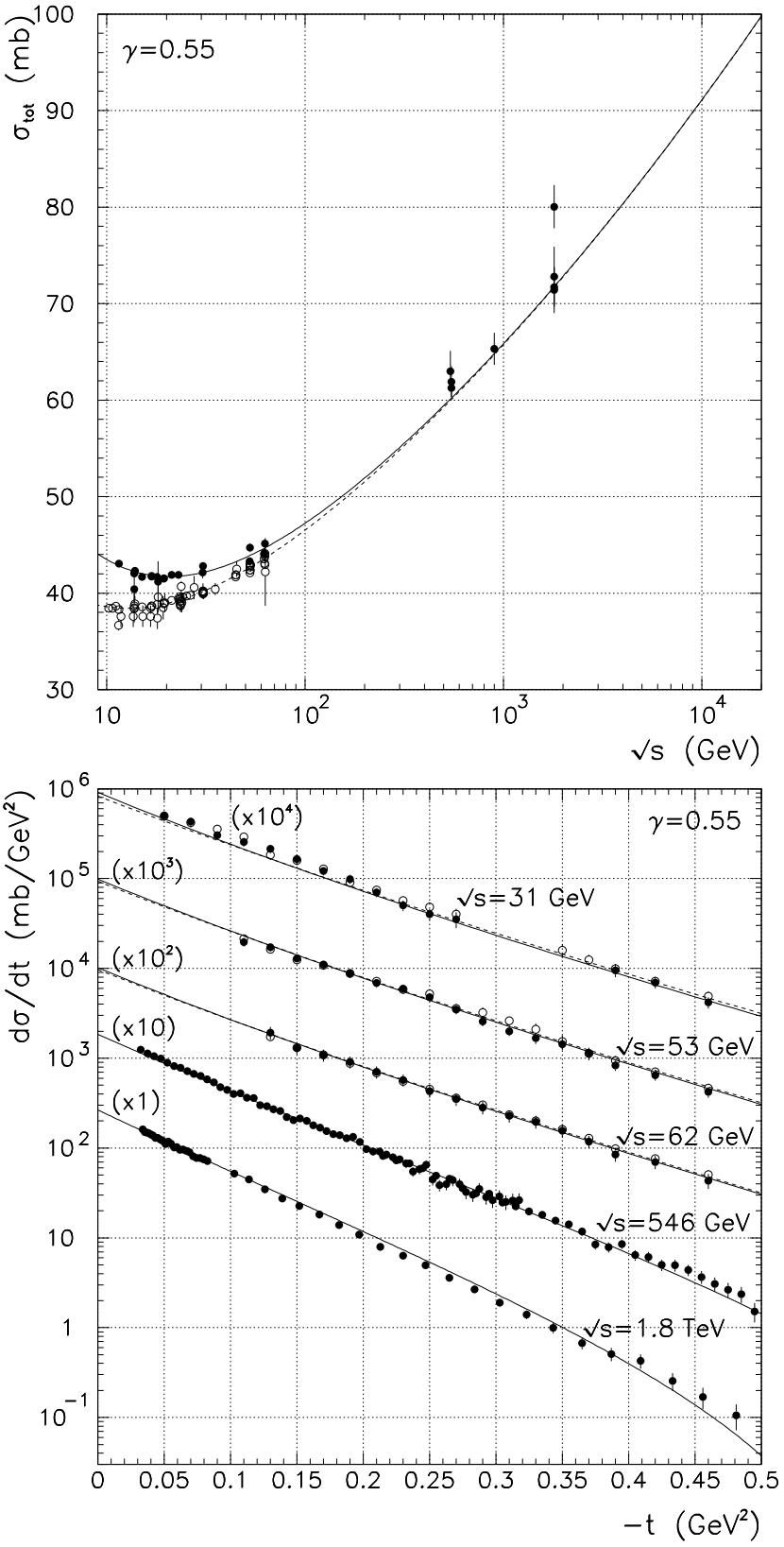

Figure 1: Two-channel eikonal model description of total and differential cross section data.

$\beta_P(0)$	2.26 ± 0.02
a_1	0.44 ± 0.01
a_2	16.3 ± 2.8
$\alpha_P(0)$	1.121 ± 0.001
α'_P	0.033 ± 0.002
$\beta_+(0)$	5.9 ± 1.2
r_+	0.5 ± 1.2
$\alpha_+(0)$	0.54 ± 0.04
$\beta_-(0)$	2.4 ± 0.9
r_-	3.1 ± 6.0
$\alpha_-(0)$	0.57 ± 0.09

Table 1: The values of the Pomeron, and the positive and negative signature secondary Reggeon parameters obtained in the fit to the total and elastic differential cross section pp and $p\bar{p}$ data. GeV units are used; so, for example, the couplings $\beta(0)$ have units of GeV^{-1}. The couplings $\beta_i(0)$ that we quote are actually $\mathrm{Im}(\eta_i\beta_i(0))$, where the signature factor η_i is given by (17), see the last paragraph of Section 2.1. The errors correspond to a 90% confidence level.

4 High-mass diffraction: triple-Regge formalism

The multichannel eikonal is unable to account for diffraction into high mass states. These processes, $pp \to pX$ with large M_X, are usually described in terms of a triple-Regge formalism, where

$$M_X^2 \;\simeq\; (1-x_L)s, \tag{32}$$

where $x_L \equiv 1-\xi$ is the momentum fraction of the ingoing proton carried by the outgoing proton. The approach is sketched in Fig. 2. Since we have large M_X we no longer have

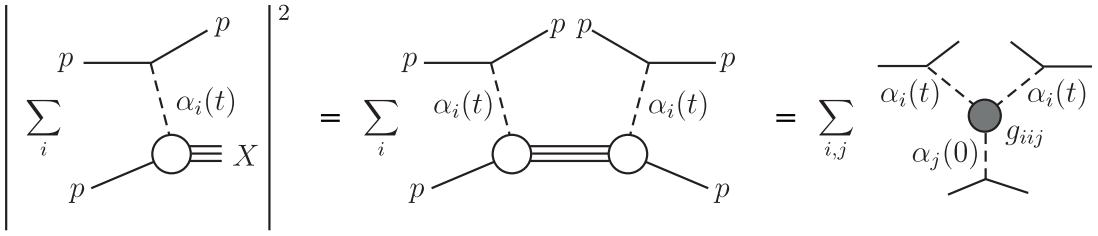

Figure 2: The triple-Regge description of high-mass diffractive dissociation, $pp \to pX$. In general, we may have vertices with three different Reggeons with coupling $g_{ii'j}$. However, here it is sufficient to consider only contributions with $i = i'$.

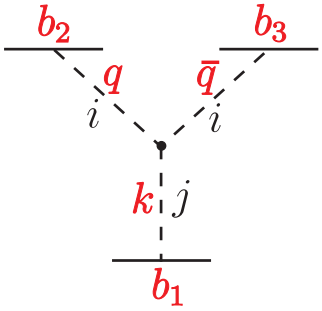

Figure 3: A schematic diagram showing the notation of the impact parameters arising in the calculation of the screening corrections to the iij triple-Regge diagram. The conjugate momenta to b_1, b_2, b_3 are $k_t, q_t, \bar{q}_t$. If $k_t = 0$, then $\bar{q}_t = q_t$.

$-t = q_t^2$. Rather, we must allow for non-vanishing $t_{\rm min}$

$$-t \;=\; \frac{q_t^2}{x_L} + \frac{m_p^2(1-x_L)^2}{x_L} \;=\; \frac{q_t^2}{x_L} - t_{\rm min}. \tag{33}$$

To the best of our knowledge, the screening corrections have not been explicitly included in the triple-Regge formalism. Therefore we present the formalism below, first using a single-channel eikonal and then generalising it to the two-channel case. Finally we treat the corrections to the $\pi\pi P$ diagram as a special case.

4.1 Screening corrections in the triple-Regge formalism

If we first neglect the screening correction, then the iij triple-Regge diagram of Fig. 2 gives the contribution

$$\frac{M^2 d\sigma}{dt dM^2} \;=\; \beta_j(0)\beta_i^2(t) g_{iij}(t) \left(\frac{s}{M^2}\right)^{2\alpha_i(t)-2} \left(\frac{M^2}{s_0}\right)^{\alpha_j(0)-1}. \tag{34}$$

We use a simple exponential parametrisation of the triple-Regge vertices

$$g_{iij}(t) \;=\; g_{iij}(0)\, \exp(b'_{iij}(q^2 + \bar{q}^2 - k_t^2)), \tag{35}$$

where the momenta are defined in Fig. 3, and where $q^2 = t_{\rm min} - q_t^2/x_L$.

Screening effects are best included by working in impact parameter space and using suppression factors of the form $\exp(-\Omega(b))$. To determine the q_t or t dependence we take the Fourier transforms with respect to the impact parameters specified in Fig. 3. We obtain[10]

$$\frac{M^2 d\sigma}{dt dM^2} \;=\; A \int \frac{d^2b_2}{2\pi} e^{i\vec{q}_t\cdot\vec{b}_2} F_i(b_2) \int \frac{d^2b_3}{2\pi} e^{i\vec{q}_t\cdot\vec{b}_3} F_i(b_3) \int \frac{d^2b_1}{2\pi} F_j(b_1), \tag{36}$$

[10]Note that $e^{i\vec{k}_t\cdot\vec{b}_1} = 1$ as $k_t = 0$.

where

$$F_i(b_2) \;=\; \frac{1}{2\pi\beta_i(q_t=0)}\int d^2q_t\beta_i(q_t)\left(\frac{s}{M^2}\right)^{-\alpha_i' q_t^2} e^{b'_{iij}q^2}e^{i\vec{q}_t\cdot\vec{b}_2}, \tag{37}$$

$$F_j(b_1) \;=\; \frac{1}{2\pi\beta_j(k_t=0)}\int d^2k_t\beta_j(k_t)\left(\frac{M^2}{s_0}\right)^{-\alpha_j' k_t^2} e^{-b'_{iij}k_t^2}, \tag{38}$$

and where the q_t-independent factors are collected in A

$$A \;=\; \beta_j(0)\beta_i^2(0)g_{iij}(0)\left(\frac{s}{M^2}\right)^{2\alpha_i(t_{\min})-2}\left(\frac{M^2}{s_0}\right)^{\alpha_j(0)-1}. \tag{39}$$

These equations assume that we have a strong triple-Pomeron scenario, see (4). For the weak triple-Pomeron coupling ansatz, (2), we must include a factor q_t in the integrand of the expression (37) for $F_i(b_2)$ when $i,j=P$, and also $\bar{q}_t$ $(=q_t)$ in the analogous formula for $F_i(b_3)$.

To include the screening corrections, for a single-channel eikonal, we must include in the integrands on the right-hand side of (36) the factors

$$\exp(-\Omega(\vec{b}_2-\vec{b}_1)/2)\,\exp(-\Omega(\vec{b}_3-\vec{b}_1)/2) \;\equiv\; S(\vec{b}_2-\vec{b}_1)\;S(\vec{b}_3-\vec{b}_1). \tag{40}$$

That is, we need to compute

$$\left.\frac{M^2 d\sigma}{dtdM^2}\right|_{iij} \;=\; A\int\frac{d^2b_1}{2\pi}F_j(b_1)|I_d(b_1)|^2, \tag{41}$$

where I_d is given by

$$I_d(b_1) \;\equiv\; \int\frac{d^2b_2}{2\pi}e^{i\vec{q}_t\cdot\vec{b}_2}F_i(b_2)S_i(\vec{b}_2-\vec{b}_1). \tag{42}$$

4.2 Generalisation to a two-channel eikonal

Recall that in the two-channel eikonal, we take the Pomeron couplings to each diffractive eigen component k to be[11]

$$\beta_{P,k}(t) \;=\; (1\pm\gamma)\beta_P(t). \tag{43}$$

On the other hand, for the secondary Reggeons, R, which are believed to dominantly couple to valence quarks, we take

$$\beta_{R,k}(t) \;=\; \beta_R(t), \tag{44}$$

that is, the same β_R for each component. Thus for the PPP, RRP and $\pi\pi P$ couplings (with $j=P$) we make the replacement

$$|I_d|^2 \;\;\to\;\; [(1+\gamma)|I_p|^2+(1-\gamma)|I_m|^2]/2 \tag{45}$$

[11] Following [14], we assume the same structure, that is the same shape and size for each component, apart, of course, from the cross section.

in (41), whereas for the PPR and RRR (with $j = R$) we let

$$|I_d|^2 \;\;\rightarrow\;\; [|I_p|^2 + |I_m|^2]/2. \tag{46}$$

The subscripts p, m are used to denote the $(1 \pm \gamma)$ eigen components respectively. In addition for I_p we replace S_i, with $i = P$, in (42) by

$$S_i \;\;\rightarrow\;\; S_{pP} \;=\; \frac{1}{2}\left[(1+\gamma)e^{-(1+\gamma)^2\Omega/2} + (1-\gamma)e^{-(1-\gamma^2)\Omega/2}\right] \tag{47}$$

and for I_m

$$S_i \;\;\rightarrow\;\; S_{mP} \;=\; \frac{1}{2}\left[(1+\gamma)e^{-(1-\gamma^2)\Omega/2} + (1-\gamma)e^{-(1-\gamma)^2\Omega/2}\right]. \tag{48}$$

These replacements of S_i are for the PPP and PPR contributions. For the RRP, $\pi\pi P$ and RRR contributions, with $i = R$ or π, we have

$$S_i \;\;\rightarrow\;\; S_{pR} \;=\; \frac{1}{2}\left[(e^{-(1+\gamma)^2\Omega/2} + e^{-(1-\gamma^2)\Omega/2}\right] \tag{49}$$

$$S_i \;\;\rightarrow\;\; S_{mR} \;=\; \frac{1}{2}\left[e^{-(1-\gamma^2)\Omega/2} + e^{-(1-\gamma)^2\Omega/2}\right]. \tag{50}$$

4.3 The screening of the $\pi\pi P$ contribution

We treat the $\pi\pi P$ contribution as a special case due to the presence of the π spin-flip amplitude. First, neglecting screening, we have

$$\frac{M^2 d\sigma}{dt dM^2} \;=\; \frac{G^2_{\pi\pi N}}{4\pi}\frac{-t}{(t-m_\pi^2)^2}\beta_P(0)g_{\pi\pi P}\left(\frac{s}{M^2}\right)^{2\alpha_\pi(t)-2}\left(\frac{M^2}{s_0}\right)^{\alpha_P(0)-1}, \tag{51}$$

where $G^2_{\pi\pi N}/4\pi = 13.75$ [25]. Since the pion is almost on-mass-shell, we expect $g_{\pi\pi P} \simeq \frac{2}{3}\beta_P(0)$, according to the additive quark model. In other words

$$g_{\pi\pi P}/\beta_P(0) \;\simeq\; \sigma(\pi p)/\sigma(pp). \tag{52}$$

The factor $-t$ in (51) is given by

$$-t \;=\; q_t^2 + q_\parallel^2 \;=\; q_t^2 + q_t^2\frac{1-x_L}{x_L} + \frac{m_p^2(1-x_L)^2}{x_L}, \tag{53}$$

where the $q_t^2 = (\vec{q}_t \cdot \vec{\sigma})^2$ term is of proton spin-flip (sf) origin, and the remaining two terms are spin non-flip. Here, $\vec{\sigma}$ is the Pauli matrix associated with the spin of the incoming proton. The non-flip interaction, is screened in the usual way, see (45), (49) and (50). However, the spin-flip amplitude is now a *vector* directed along $\vec{q}_t$. Thus the integrals in (37) and (42) should be written in vector form, with

$$\frac{\beta_\pi^{\rm sf}(q_t)}{\beta_\pi^{\rm sf}(q_t=0)} \;=\; \frac{\vec{q}_t}{t-m_\pi^2}, \tag{54}$$

and $(\beta_\pi^{\rm sf}(0))^2$ in (39) replaced by $G^2_{\pi\pi N}/4\pi$. This leads to

$$\vec{F}_\pi^{\rm sf}(\vec{b}_2) \;=\; \vec{b}_2 f_\pi^{\rm sf}(b_2) \tag{55}$$

and

$$|I_d^{\rm sf}|^2 \;=\; |I_x|^2 + |I_y|^2 \tag{56}$$

with x directed along $\vec{q}_t$. After the azimuthal integration, it means that the Bessel function $J_0(qb)$, that arises in (37), should be replaced by $J_1(qb)$.

5 Triple-Regge analysis of $pp \to pX$ and $\bar{p}p \to \bar{p}X$ data

The main objective of this paper is to perform a triple-Regge analysis of the available $d^2\sigma/dtd\xi$ data for $pp \to pX$ and $\bar{p}p \to \bar{p}X$ (where $\xi = M_X^2/s$), allowing for screening (that is absorptive) effects. In this way we obtain a more reliable estimate of the *bare* triple-Pomeron coupling, g_{PPP}, which is a vital ingredient in the description of diffractive processes at high energy, see Ref. [12, 13, 26]. As can be seen from the triple-Regge formalism of the previous section, it is necessary to work in impact parameter space in order to include screening corrections. However, it is computationally time-consuming to evaluate the required Fourier transforms inside a χ^2 fit. To facilitate the fit to the data, we therefore first prepare grids of the integral in (41) for a range of fixed values of the slopes b'_{iij} of the triple-Regge vertices for each q_t and M^2 data point. A MINUIT fit to the data is then performed using Chebyshev polynomial interpolation in b'_{iij}.

In fact, we performed three triple-Regge fits to the $d^2\sigma/dtd\xi$ data with different assumptions for the form of the triple-Pomeron vertex. The first two assume either a strong or weak coupling triple-Pomeron vertex, that is they correspond to

$$g_{3P}^S(0) \qquad \text{and} \qquad g_{3P}^W(0) q_t^2 \exp(-b' q_t^2) \tag{57}$$

respectively, see (4) and (2); recall that we use GeV units. The third fit considers a combination of the two couplings with both $g_{3P}^S(0)$ and $g_{3P}^W(0)$ as free parameters.

We fit to CERN-ISR[12] [27], FNAL fixed-target [28] and Tevatron [29] data for $pp \to pX$ and $\bar{p}p \to \bar{p}X$. The differential distributions for the FNAL fixed target and Tevatron experiments can be found in Ref. [9]. The relative normalisations of the data sets are not very well known. In Ref. [9] it was claimed that the normalisation uncertainties of the FNAL data are about 10%. We fix the normalisation of the ISR data and introduce normalisation factors for the FNAL data with a 10% error. However, we find that the Tevatron data prefer to be normalised up by the strong coupling fit, and down for the weak coupling fit, by factors of about 25%. We restrict this freedom and limit the normalisation factors to $\pm 15\%$ and $\pm 10\%$ for $\sqrt{s} = 546$ and 1800 GeV data respectively, where the + and − signs refer to the strong and weak coupling fits

[12] We choose a subset of the ISR data which is sufficient to fully describe their t and ξ dependence.

respectively. The remaining normalisations coming from the fits are +10% for the $\sqrt{s} = 14,\ 20$ GeV data [28].

All three fits to the data prefer very small, or even negative, slopes, b'_{iij}, of the triple-Regge vertices. To avoid unphysical negative slopes, we impose the condition that $b'_{iij} > 0$. In fact, the optimum χ^2 for each fit has, within error bars, all $b'_{iij} = 0$. Therefore, for the couplings quoted in Table 2, we have set all the slopes $b'_{iij} = 0$. The only exceptions to this are the slopes of the PPP and PPR vertices for the weak coupling fit, which are found to be positive, as shown in Table 2. We fixed the $\pi\pi P$ triple coupling at the additive quark model value, $g_{\pi\pi P} = \frac{2}{3}\beta_P(0)$. Actually the data prefer a smaller value, but with a large error. However the fixed value of $g_{\pi\pi P}$ only enlarges χ^2 by less than 0.5. The couplings of the Reggeons to the proton are taken from the "elastic" analysis of Section 3. The values of the remaining parameters, corresponding to the optimum triple-Regge fits, are given in Table 2.

	strong	weak	combination
g^S_{3P}	0.44 ± 0.05	-	0.44 ± 0.10
g^W_{3P}	-	3.0 ± 1.2	0.2 ± 0.5
b'^W_{PPP}	-	1.15 ± 0.3	-
g_{PPR}	0.75 ± 0.10	0.76 ± 0.15	0.67 ± 0.16
b'^W_{PPR}	-	1.4 ± 1.7	-
g_{RRP}	1.1 ± 0.3	1.3 ± 0.5	1.0 ± 0.5
g_{RRR}	2.6 ± 1.0	2.9 ± 1.4	2.8 ± 1.5
χ^2/DoF	0.83	1.40	0.83

Table 2: The values of the *"bare"* triple-Regge couplings $g_{iij}(0)$ of (39), and slopes b'_{iij} of (37, 38), obtained in the three optimum fits to the $d^2\sigma/dtd\xi$ data. Recall that all the slopes b'_{iij} are set to zero, except for those of the PPP and PPR vertices in the weak coupling fit.

We see from the χ^2 per degree of freedom (DoF) that the data clearly prefer the *strong*, rather than the *weak*, triple-Pomeron coupling ansatz. This is also clear from the "weak+strong combination" fit, which is dominated by the strong coupling component, and is little changed from the pure strong coupling fit[13]. The preference for the strong triple-Pomeron coupling is also evident from Fig. 4. This compares the "strong" and "weak" descriptions of a sample of the $d^2\sigma/dtd\xi$ data that are fitted, including especially the high energy FNAL data at $\sqrt{s} =$ 546 and 1800 GeV. The FNAL data are most relevant since the triple-Pomeron contribution dominates for $\xi \lesssim 0.03$. We see that the weak coupling description of the ξ shape of these data is disfavoured.

The t-dependence of the single diffractive cross section, $d^2\sigma/dtd\xi$, is shown, for example, in Fig. 5 for $\xi = 0.01,\ 0.1$ at $\sqrt{s} = 1800$ GeV, and in Fig. 6 for $\xi = 0.02,\ 0.06$ at the much lower

[13]The normalisations of the data that are found in the "combination" fit are the same as those of the strong coupling fit.

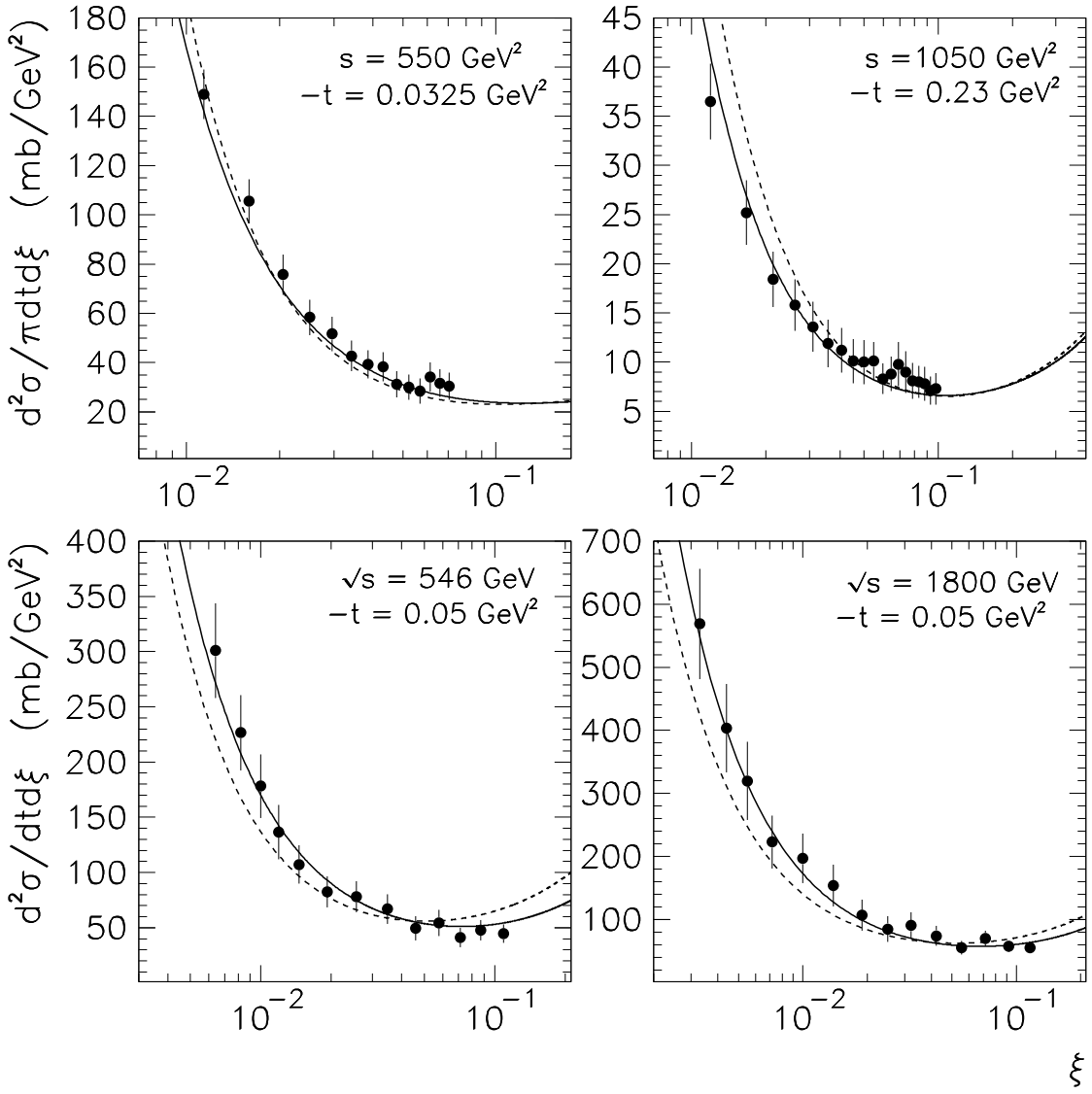

Figure 4: The description of a sample of the $d^2\sigma/dtd\xi$ cross section data that are fitted using the strong (continuous curves) and weak (dashed curves) triple-Pomeron coupling ansatzes. ($\xi \simeq M^2/s$). Here, the curves corresponding to the (strong, weak) coupling fits of the FNAL data have been normalised (down, up) by 15% at $\sqrt{s} = 546$ GeV and by 10% at $\sqrt{s} = 1800$ GeV, to allow for the normalisations found for these data in the respective fits.

energy corresponding to $s = 550$ GeV^2. We also show the individual triple-Regge contributions in these plots, together with the data available at these kinematic values. Note that, after accounting for the absorptive effects, the triple-Pomeron contribution does not vanish in the forward direction even in the *weak* coupling fit. Therefore to choose between the *weak* and *strong* coupling scenarios we have had to perform a full fit of the data. It is not enough just to study the low q_t behaviour of the cross section. The first indication of the weak coupling characteristics is seen in Fig. 5 for $\xi \sim 0.01$ and $|t| < 0.1$ GeV^2 at the Tevatron energy. In this domain the data favour the strong coupling scenario. For larger values of ξ the dip produced by the PPP term in the weak coupling case is filled in by the peak due to the $\pi\pi P$ term. At the lower energy, corresponding to 550 GeV^2, we see, from Fig. 6, that it is difficult to distinguish between the two scenarios. However, at the higher energy of the LHC the weak coupling scenario will reveal itself by a well pronounced dip at $t \simeq -0.02$ GeV^2 after which $d^2\sigma/dtd\xi$ increases with $|t|$ up to $|t| \simeq 0.15$ GeV^2, see Fig. 7. It is clear from Fig. 7 that single diffractive dissociation data obtained at the LHC for $\xi \sim 0.01$ should be able to readily distinguish between the strong and weak triple-Pomeron coupling scenarios.

In the remainder of this Section, we discuss only the favoured strong triple-Pomeron coupling fit, for which the triple-Regge couplings are the first set listed in Table 2. The values of these couplings are rather stable. They never go outside the quoted errors when we change the renormalisation parameters of the data, or allow $g_{\pi\pi P}$ to be a free parameter. The quality of the fit is excellent, with a minimum $\chi^2/\text{DoF} = 167/(210-8) = 0.83$. The 8 parameters are the 4 couplings, $g_{iij}(0)$, and the 4 data renormalisations. The quality of the description can been seen from the plots of samples of the data that are fitted, Fig. 8 and Fig. 9, which also show the various triple-Regge contributions to the cross section.

In comparison with the old triple-Regge analysis of Ref. [6], we now obtain a more than twice larger relative contribution of the PPR term. This is mainly due to the inclusion in our analysis of the higher energy Tevatron data. The inclusive cross sections measured in the interval of $\xi \sim 0.01 - 0.03$ at the Tevatron energies turn out to be about twice smaller than that measured at the low CERN-ISR energies.

The "strong coupling" parameters of Table 2 are much closer to the *bare* triple-Reggeon couplings than those coming from the old fits [5, 6, 7] which did not allow for the screening corrections. In particular the value[14].

$$g_{3P} \equiv g_{PPP} \simeq 0.2\,\beta_P \tag{58}$$

is consistent with the reasonable extrapolation of the perturbative BFKL Pomeron vertex to the low scale region [30]. However, these are still not the true bare vertices. For these sizeable values of g_{iij} the effect of "enhanced" screening, shown in Fig. 10, is not negligible. Moreover, it is not enough to just take one iteration, that is, to repeat the "elastic" analysis, but now including the

[14]Note that this result is in reasonable agreement with the parametrisation of the renormalised triple-Pomeron amplitude of Ref. [9] which leads to $g_{3P} \simeq 0.15\,\beta_P$

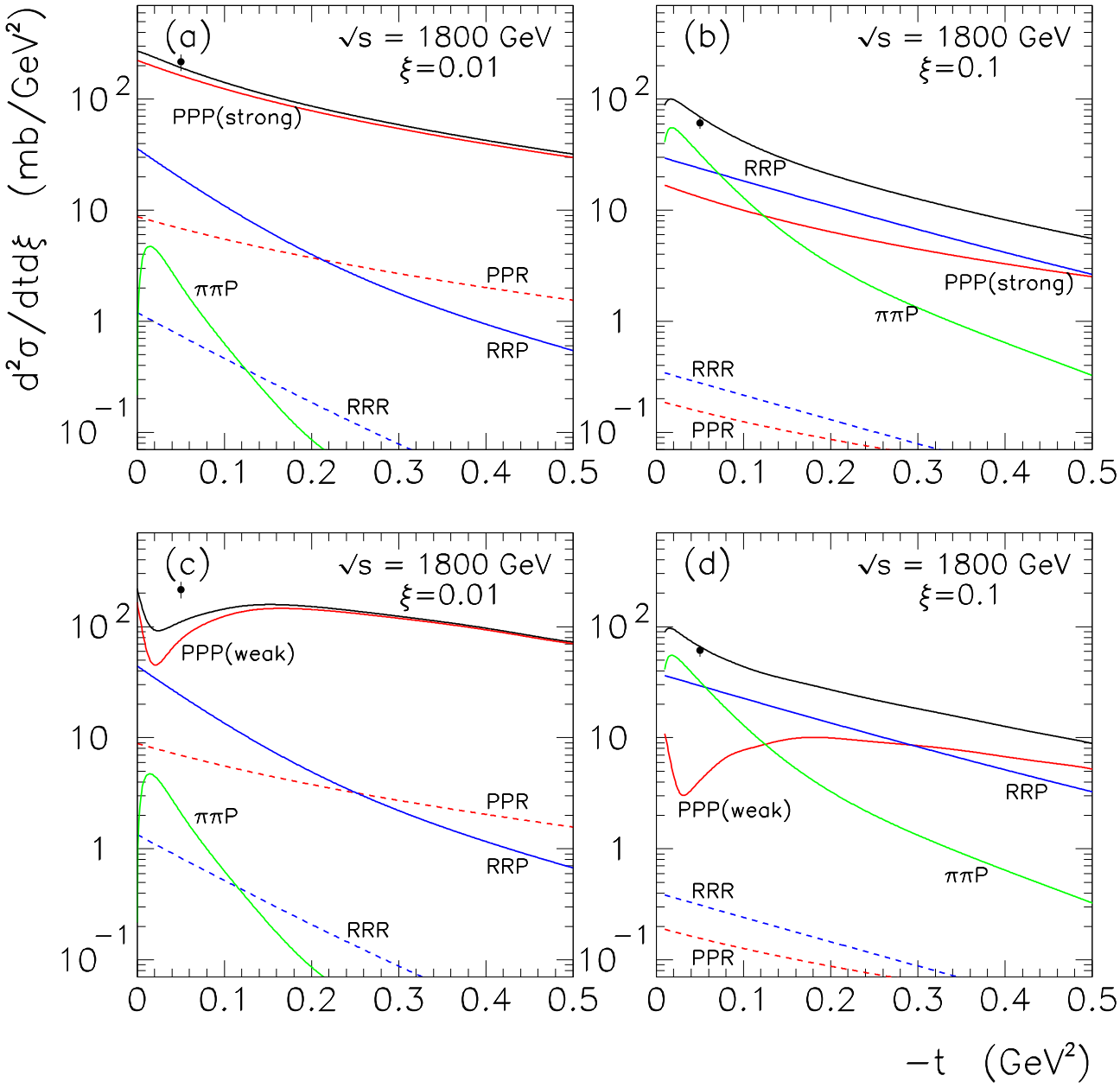

Figure 5: The four plots show the t-dependence of the $d^2\sigma/dtd\xi$ at $\xi = 0.01,\ 0.1$ and $\sqrt{s} = 1800$ GeV obtained in the strong and weak triple-Pomeron fits respectively.

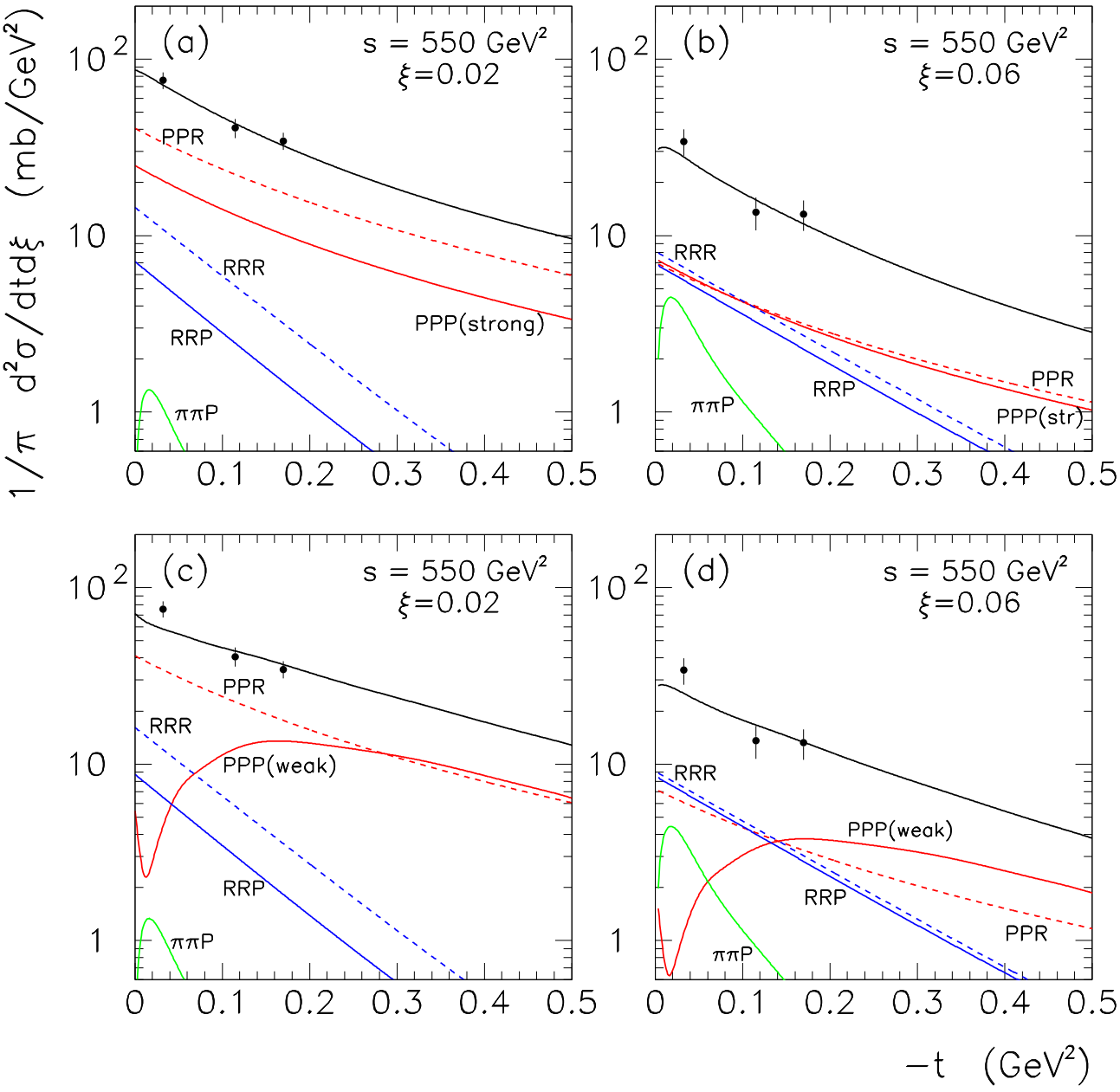

Figure 6: The four plots show the t-dependence of the $d^2\sigma/dtd\xi$ at $\xi = 0.02,\ 0.06$ and $s = 550\ \mathrm{GeV}^2$ obtained in the strong and weak triple-Pomeron fits respectively, together with the data available at these kinematic values.

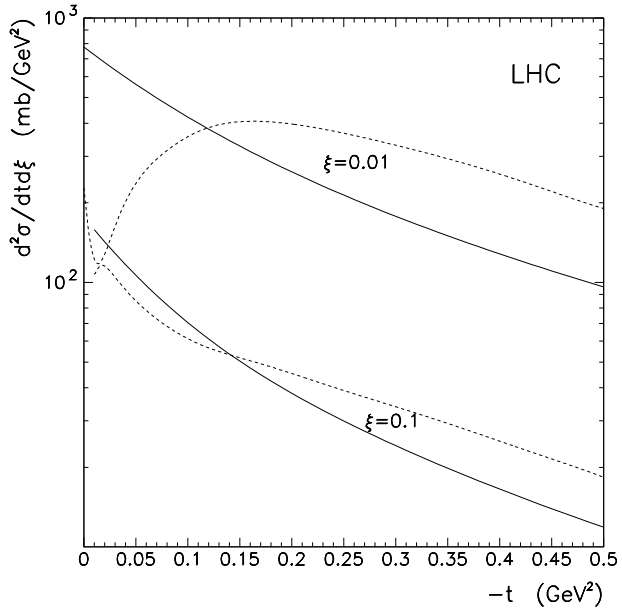

Figure 7: The continuous curves are the predictions for the t-dependence of the $d^2\sigma/dtd\xi$ at $\xi = 0.01,\ 0.1$ and $\sqrt{s} = 14$ TeV obtained in the strong triple-Pomeron fit. The disfavoured weak coupling predictions are shown by dashed curves.

effects of the triple-Regge high-mass absorption, obtain new Regge-proton parameters and then repeat the triple-Regge analysis[15]. Rather, it is necessary to sum up the series of multi-Reggeon diagrams. We have considered such a model [23], that is an extension of an earlier model [3] but now including non-zero α'_P as a free parameter, as well as more t-channel exchanges. The tuning of this model shows that it is possible to obtain a good description of the data provided that the triple-Pomeron coupling is a bit larger

$$g_{3P} \ \simeq \ 0.25\ \beta_P. \tag{59}$$

6 Inelastic J/ψ photoproduction

In Ref. [26] it was pointed out that the observation of the process $\gamma p \to J/\psi + Y$ at large values of M_Y offers, in principle, an opportunity to determine the triple-Pomeron coupling where the screening corrections are smaller than in the pure hadronic reactions, see also [32]. Unfortunately, the M_Y^2 distribution has not been measured yet. However there exists a comparison of the HERA data for the "elastic" photoproduction process, $\gamma p \to J/\psi + p$ with the proton

[15]Note that an eikonal-type model for absorption will still violate s-channel unitarity [31]. At large b, on the periphery, where the opacity $\Omega(b)$ is small, the effect of eikonal screening is not effective. For these (large l) partial waves the contribution coming from diffractive dissociation becomes larger than the total inelastic contribution. To satisfy unitarity more complicated (enhanced) multi-Pomeron diagrams must be included.

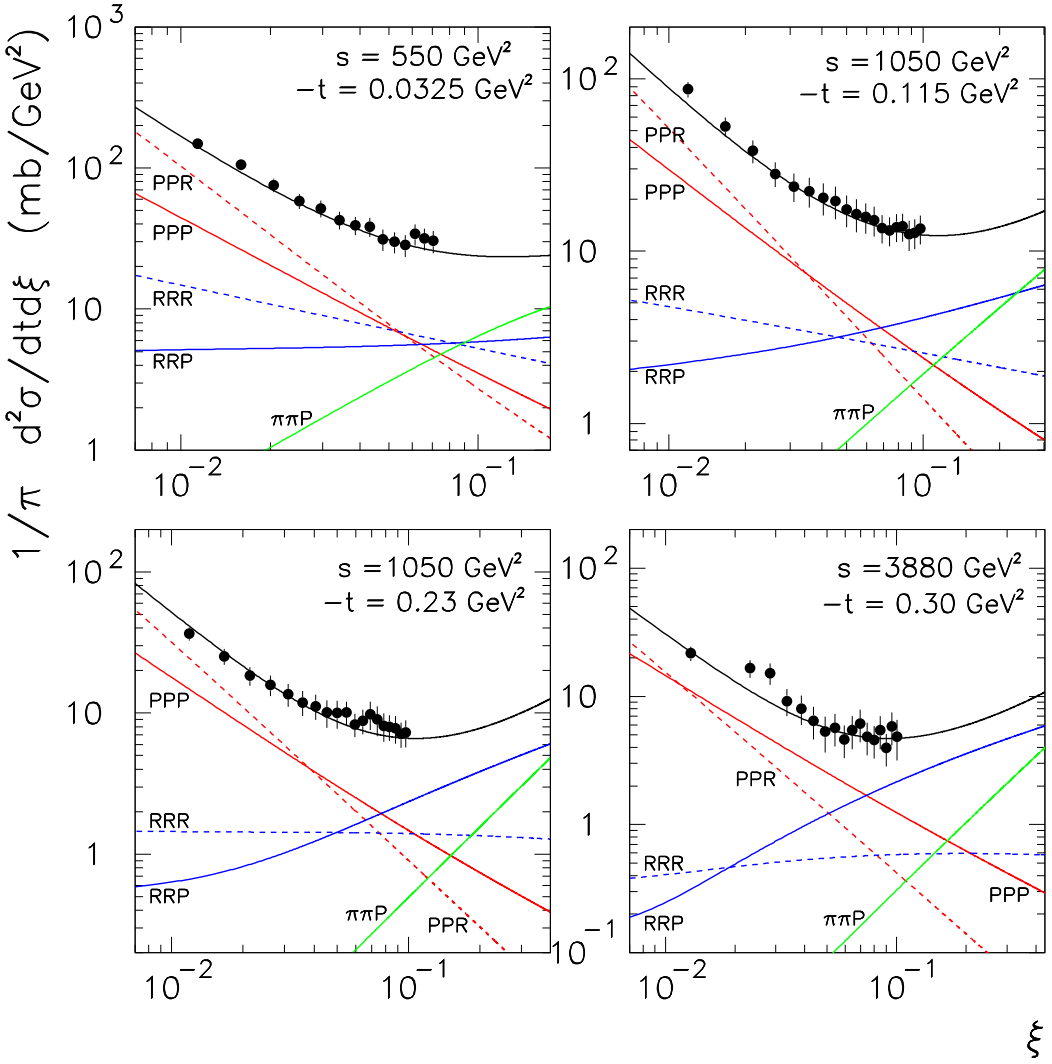

Figure 8: The description of the CERN-ISR $pp \to pX$ cross section, $d^2\sigma/dtd\xi$, data [27] obtained in the strong triple-Pomeron coupling fit. ($\xi \simeq M^2/s$). The individual triple-Regge contributions are also shown.

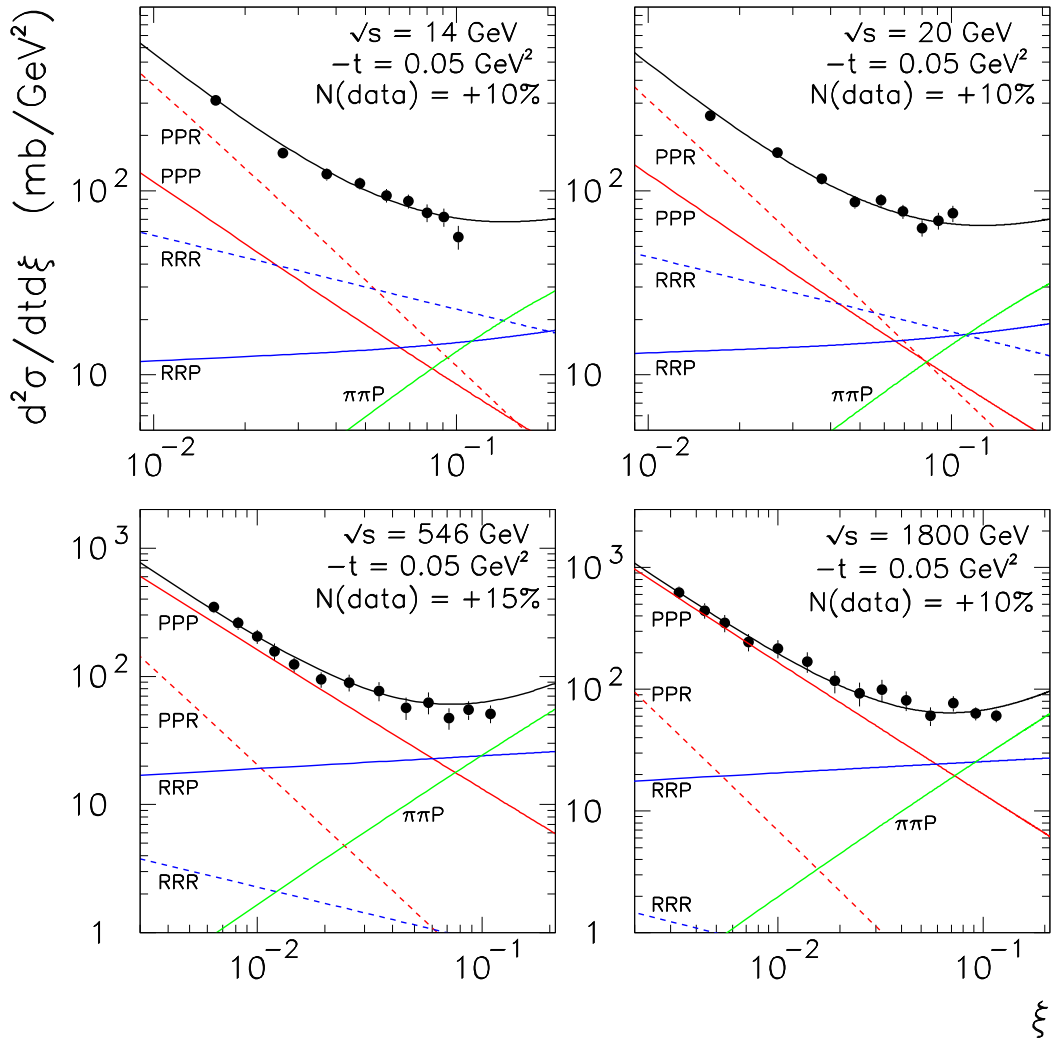

Figure 9: The description of the $d^2\sigma/dtd\xi$, measured in fixed-target and collider experiments at FNAL [28, 29, 9], obtained in the strong triple-Pomeron coupling fit. The individual triple-Regge contributions are also shown.

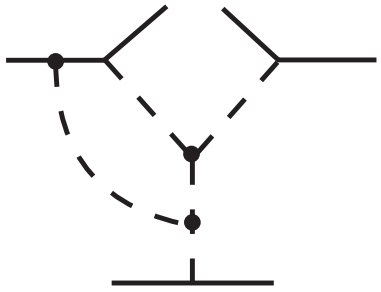

Figure 10: An example of an "enhanced" contribution to high-mass diffraction.

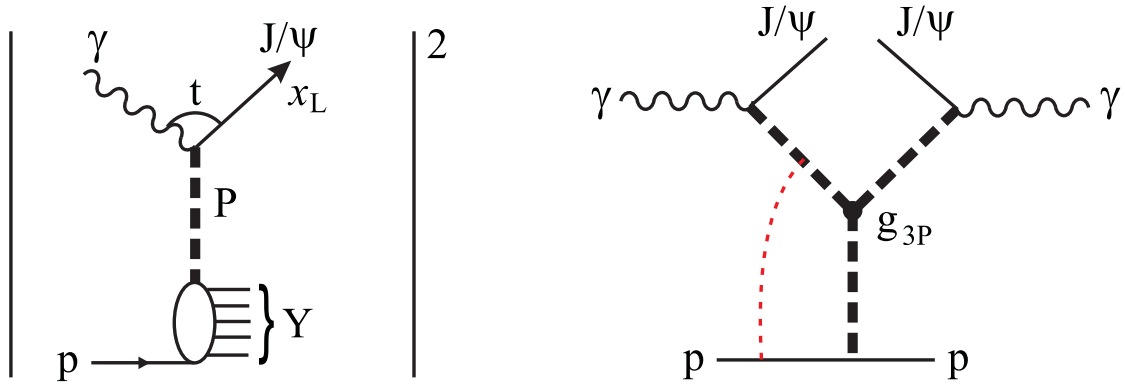

Figure 11: The process of proton dissociation in diffractive J/ψ photoproduction, $\gamma+p \to J/\psi+Y$, which is described by a diagram with a triple-Pomeron vertex in which the rescattering effects are small. The dotted line would mean the diagram became an enhanced diagram. This contribution is small.

dissociation data. The ratio, at the photon-proton centre-of-mass energy $W = 200$ GeV and $t = 0$, is [33]-[37].

$$r \equiv \frac{d\sigma(\gamma p \to J/\psi + Y)/dt}{d\sigma(\gamma p \to J/\psi + p)/dt} \simeq 0.2, \tag{60}$$

where the "inelastic" cross section has been integrated over the mass region $M_Y < 30$ GeV. Since only the Pomeron couples to charm quarks, the ratio r is described by the PPP and PPR contributions. The cross section for J/ψ absorption is rather small. So we may neglect the screening factor, and obtain

$$r = \frac{1}{\pi\beta_P(0)} \int \frac{dM^2}{M^2} \left(\frac{s_0}{M^2}\right)^{2\hat{\alpha}_P - 2} \left[g_{PPP} \left(\frac{M^2}{s_0}\right)^{\alpha_P(0)-1} + g_{PPR} \frac{\beta_{f_2}(0)}{\beta_P(0)} \left(\frac{M^2}{s_0}\right)^{\alpha_R(0)-1} \right]. \tag{61}$$

Note that the Pomeron trajectories $\alpha_P(0)$ and $\hat{\alpha}_P(t)$ in (61), that is in the triple-Pomeron diagram in Fig. 11, are not the same. The lower Pomeron $\alpha_P(0)$ in Fig. 11 is the usual 'soft'

Pomeron; whereas the upper ones, with $\hat{\alpha}_P(t)$, include DGLAP evolution from a low initial scale $\mu = \mu_0$ up to a rather large scale $\mu \sim M_{J/\psi}$ at the J/ψ production vertex. The summation of the double logarithms $(\alpha_s \ln(1/x) \ln(\mu^2/\mu_0^2))^n$ leads to a steeper x-dependence and hence to a larger effective intercept for the trajectory $\hat{\alpha}_P(t)$ of the upper 'hard' Pomeron. Thus to evaluate the ratio r of (61) we take $\hat{\alpha}_P = 1.18$, which corresponds to the W dependence observed in the HERA data [34]-[37]. Taking the other parameters from Table 1 and the strong coupling fit of Table 2, we obtain for the two terms in (61)

$$r \;\equiv\; r_{PPP} + r_{PPR} \;=\; 0.12 + 0.06. \tag{62}$$

This is consistent with the HERA data, within the uncertainties.

We also use the weak triple-Pomeron coupling fit of Table 2 to evaluate the ratio r at $t = -0.2$ GeV^2. This is the lowest $-t$ value for which r is measured. The experimental value is[16] [33]

$$r \;=\; 0.4 \pm 0.1, \qquad \text{for} \;\; t = -0.2 \text{ GeV}^2. \tag{63}$$

When we evaluate the weak PPP coupling and PPR contributions to r, we find

$$r \;\equiv\; r_{PPP} + r_{PPR} \;=\; 0.14 + 0.07, \qquad \text{for} \;\; t = -0.2 \text{ GeV}^2, \tag{64}$$

a value about a factor two smaller than that observed. So again the strong triple-Pomeron coupling is favoured over the weak.

Originally, the strong triple-Pomeron coupling was supported by an analysis [26] of the HERA J/ψ photoproduction data. The problem is that, at present, the M_Y^2 dependence of the cross section has not been measured; only the value integrated over an M_Y^2 interval is given. The large value of the triple-Pomeron coupling that was extracted in [26] assumed that the whole cross section originates from Pomeron exchange, and neglected the secondary Reggeon contribution. Here we have included the secondary Reggeon contribution. However, if the M_Y^2 distribution were to be observed, it would then be possible to separate these contributions using just the J/ψ photoproduction data, and to give an independent check of the results of our triple-Regge analysis. Clearly a dedicated measurement of the process $\gamma p \to J/\psi + Y$, including especially the M_Y and t dependence, would be extremely informative.

7 Conclusions

We have performed a triple-Regge analysis of the available $pp \to p + X$ and $\bar{p}p \to \bar{p} + X$ data, in which we account for absorptive effects. Thus, the couplings of the triple-Reggeon vertices extracted in this analysis will be much closer to the couplings of the original *bare* vertices than

[16] The measured ratio at $t = -0.2$ GeV^2 is larger than that of (60) at $t = 0$, since the cross section of the elastic process, $\gamma p \to J/\psi + p$, has a larger t-slope than that for $\gamma p \to J/\psi + Y$.

those obtained in the old analyses, where the screening corrections were implicitly included in the values of *effective* couplings.

The triple-Pomeron vertex turns out to be rather large, $g_{3P} \simeq 0.2\beta_P$. This indicates that, in a more precise description of "soft" interactions, we must include more complicated 'enhanced' diagrams and diagrams with the multi-Pomeron vertices (that is with a larger number of Pomerons in a vertex).

Due to the inclusion of the high-energy Tevatron data in the analysis, we now obtain a twice larger relative contribution of the PPR term in comparison with the results of the old analyses.

We considered two possible parametrisations of the small q_t behaviour of the triple-Pomeron vertex:

$$g_{3P} = \text{constant} \qquad \text{and} \qquad g_{3P} = g^W_{3P}(0) q_t^2 \exp(-b' q_t^2), \tag{65}$$

in GeV units. We found that the data prefer the first, the so-called *strong* Pomeron coupling scenario. In the second, the so-called *weak* coupling, case, we obtained a much poorer description of the high-energy Tevatron (CDF) data at small ξ and low $-t = 0.05$ GeV^2, where the triple-Pomeron contribution dominates. It will be important to measure the inclusive cross section for single diffraction, $d^2\sigma/dtd\xi$, at the LHC to confirm this conclusion. This could be done when the forward detectors are operating at the LHC, even at moderate integrated luminosity [38]. Another possibility is to study in more detail J/ψ diffractive production with dissociation of the target proton. That is, to measure the M_Y^2 and t dependence of the $\gamma p \to J/\psi + Y$ reaction. The HERA experiments have so far only presented the cross section integrated over M_Y^2 up to $M_Y = 30$ GeV. However, already these data support the *strong* coupling solution.

Finally, we note that our analysis of the data prefers zero slopes, corresponding to small size of the bare triple-Reggeon vertices. Together with the larger values of the PPP and PPR vertices, this gives hope that there is a smooth matching to the perturbative QCD treatment of the Pomeron.

Acknowledgements

We thank Aliosha Kaidalov, Alessia Bruni and Risto Orava for useful discussions. MGR and EGSL thank the IPPP at the University of Durham for hospitality. The work was supported by INTAS grant 05-103-7515, by grant RFBR 07-02-00023, by the Russian State grant RSGSS-3628.2008.2 and by the CNPq (Brazil) under contract 210242/2006-0.

References

[1] for a recent review see M. M. Block, Phys. Rept. **436**, 71 (2006).

[2] M.L. Good and W.D. Walker, Phys. Rev. **120** (1960) 1857;
E.L. Feinberg and I.Ya. Pomeranchuk, Doklady Akad. Nauk SSSR **93** (1953) 439; Suppl. Nuovo Cimento v. **III**, serie X, (1956) 652.

[3] M.G. Ryskin, A.D. Martin and V.A. Khoze, Eur. Phys. J. **C54** (2008) 199.

[4] E. Gotsman, E. Levin, U. Maor and J. S. Miller, arXiv:0805.2799 [hep-ph] and references therein.

[5] A.B. Kaidalov, V.A. Khoze, Yu.F. Pirogov and N.L. Ter-Isaakyan, Phys. Lett. **B45** (1973) 493;
A.B. Kaidalov and K.A. Ter-Martirosyan, Nucl. Phys. **B75** (1974) 471.

[6] R.D. Field and G.C. Fox, Nucl. Phys. **B80** (1974) 367.

[7] for a review see A.B. Kaidalov, Phys. Rep. **50** (1979) 157.

[8] A. Capella, J. Kaplan and J. Tran Thanh Van, Nucl. Phys. **B105** (1976) 333.

[9] K. Goulianos and J. Montanha, Phys. Rev. **D59** (1999) 114017.

[10] K. Goulianos, Phys. Lett. **B358** (1995) 379; arXiv:hep-ph/9502356.

[11] M.G. Ryskin, A.D. Martin and V.A. Khoze, in Proc. of Gribov Memorial Workshop (Budapest, May 2005), p. 115, arXiv:hep-ph/0506272.

[12] V.N. Gribov and A.A. Migdal, Sov. J. Nucl. Phys. **8** (1969) 583;
V.N. Gribov, Sov. J. Nucl. Phys. **17** (1973) 313.

[13] V.N. Gribov and A.A. Migdal, Sov. Phys. JETP **28** (1969) 784.

[14] V.A. Khoze, A.D. Martin and M.G. Ryskin, Eur. Phys. J. **C18** (2000) 167.

[15] A.B. Kaidalov, V.A. Khoze, A.D. Martin and M.G. Ryskin, Eur. Phys. J. **C21** (2001) 521.

[16] A.A. Anselm and V.N. Gribov, Phys. Lett. **B40** (1972) 487.

[17] W.-M. Yao *et al.*, J. Phys. **G33**, 1 (2006).

[18] A. Breakstone *et al.*, Nucl. Phys. **B248**, 253 (1984).

[19] M. Bozzo *et al.*, Phys. Lett. **B147**, 385 (1984).

[20] N.A. Amos *et al.*, Phys. Lett. **B247**, 127 (1990).

[21] K. Goulianos, Phys. Rept. **101** (1983) 169.

[22] L. Baksay *et al.*, Phys. Lett. **B53** (1975) 484;
R. Webb *et al.*, Phys. Lett. **B55** (1975) 331;
L. Baksay *et al.*, Phys. Lett. **B61** (1976) 405;
H. de Kerret *et al.*, Phys. Lett. **B63** (1976) 477;
G.C. Mantovani *et al.*, Phys. Lett. **B64** (1976) 471.

[23] V.A. Khoze, A.D. Martin and M.G. Ryskin, in preparation.

[24] S. Sapeta and K.J. Golec-Biernat, Phys. Lett. **B613** (2005) 154.

[25] V. Stoks, R. Timmermans and J.J. de Swart, Phys. Rev. **C47** (1993) 512;
R.A. Arndt, I.I. Strakovsky, R.L. Workman and M.M. Pavan, Phys. Rev. **C52** (1995) 2120.

[26] V.A. Khoze, A.D. Martin and M.G. Ryskin, Phys. Lett. **B643** (2006) 93.

[27] J.C.M. Armitage et al., Nucl. Phys. **B194** (1982) 365.

[28] R.L. Cool et al., Phys. Rev. Lett. **47** (1981) 701.

[29] F. Abe et al., Phys. Rev. **D50** (1994) 5535.

[30] J. Bartels, M.G. Ryskin and G.P. Vacca, Eur. Phys. J. **C27** (2003) 101.

[31] E.S. Martynov and V.S. Struminsky, Phys. Atom. Nucl **59** (1996) 1755.

[32] E. Gotsman, A. Kormilitzin, E. Levin and U. Maor, Eur. Phys. J. **C52**, 295 (2007).

[33] ZEUS collaboration: Abstract 549, Int. Europhysics Conf. on HEP, Aachen, July 2003.

[34] ZEUS collaboration: S. Chekanov et al., Nucl. Phys. **B695** (2004) 3.

[35] H1 collaboration: C. Adloff et al., Eur. Phys. J. **C10** (1999) 373.

[36] ZEUS collaboration: S. Chekanov et al., Eur. Phys. J. **C24** (2002) 345.

[37] H1 collaboration: A. Aktas et. al., Eur. Phys. J. **C46** (2006) 585.

[38] V.A. Khoze, A.D. Martin and M.G. Ryskin, Eur. Phys. J. **C55** (2008) 363.